Enlarged Range and Filter-Tuned Reception in Photonic Time-Stretched Microwave Radar

Siteng Zhang, Weiwen Zou, *Senior Member, IEEE*, Na Qian, and Jianping Chen

***Abstract*— We have previously demonstrated a photonic time-stretched coherent radar (PTS-CR) with central-frequency programmable and bandwidth-tailorable agility. The sampling bandwidth in the reception was essentially compressed by the photonic time-stretched process. However, in the PTS-CR, the reception aperture suffering dead zone was hardly tuned by the fiber delay line and the measurement range was restricted by the pulse repetition rate (PRR) of the mode-locked laser. Here, we report a novel scheme to overcome the restrictions. The reception aperture can be simply tuned by adjusting the center wavelength of an optical filter and the PRR is reduced for enlargement of the measurement range by use of a photonic switch in the transmitter. In the experiment, a tenfold enlargement of measurement range is demonstrated to identify two neighboring targets separated by ∼4 cm.**

***Index Terms*— Heterodyning, radar.**

I. Introduction

RADARS have developed for decades and raised its wide applications in target recognition, remote sensing, and imaging. The pursuits of the accurate and detailed information in the region of interests push the next generation radar to work in higher carrier frequency and wider bandwidth [1]. However, conventional microwave radar systems always operate on a specific narrow band and require up- and down-conversions [2]. The distortion at high frequency and the limitation in bandwidth make microwave components difficult to meet the demands of radar in frequency aspects [3]. Owing to the inherent characteristics of ultra-wide bandwidth, low transmission loss, and low timing jitter [4], various photonics based solutions were proposed to achieve high detection resolution and even object imaging [5]–[9]. In the pioneering demonstration [5], a photonics-based radar has been utilized in the field trial with its potential in higher frequency and lower phase noise, compared with its electronic equivalent. In the system, only the carrier frequency is generated by beating two tones of one mode-locked laser (MLL). The operation bandwidth is constrained by the repetition rate of the MLL (i.e. only hundreds of MHz). The nonlinear modulation effect of the Mach-Zehnder modulator (MZM) was proposed to produce signals with gigahertz bandwidth [7]–[9] and high resolution imaging was achieved by de-chirping the frequency difference between the reference and the echo. In contrast, the wavelength-to-time (WTT) mapping [10]–[12] can be straightforwardly used to generate the radar signal with high frequency and wide bandwidth. Most recently, we presented a photonic time-stretched coherent radar (PTS-CR) [6] with the agility of the programmable central-frequency and tailorable bandwidth, where the WTT mapping was utilized in the transmitter and the time-stretched process was employed in the receiver. The laser source of both the transmitter and receiver is the same MLL so as to ensure the radar's coherence. However, there are two drawbacks of the PTS-CR [6]. First, high pulse repetition rate (PRR) of the MLL is necessary for reception but severely restricts the ambiguity-free measurement range. Second, the fiber delay line used in the receiver has a limited length variation, which introduces the dead zone of the reception aperture for the echo modulation if there is no prior information.

In this letter, we propose a novel scheme of the photonic time-stretched microwave radar (PTS-MR) to overcome the drawbacks of the measurement range and the reception aperture. In the transmitter, the PRR is reduced tenfold by utilizing a modulator as a photonic switch and the broadband linearly chirped microwave pulse is generated by heterodyning two different dispersed optical pulses from one MLL. In the receiver, a time-stretched process with a factor of five is achieved and the reception aperture is simply tuned by adjusting the center wavelength of the optical filter. The PTS-MR operates at X band with ∼4 GHz bandwidth, corresponding to ∼4 cm detection resolution.

II. Principle and Experimental Setup

The principles of the novel scheme and the original one of the PTS-MR are compared in Fig. 1. As shown in Fig. 1(a), the original scheme [6] uses the MLL as the same optical source for microwave generation and reception. Dispersion was applied to the chirped optical pulses to extend their time duration [10]–[12]. By heterodyning two rectangular-shaped optical pulses with different dispersions in time domain, broadband linearly hirped microwave pulse was generated through opto-electronic (O/E) conversion.

Manuscript received January 29, 2018; revised April 2, 2018; accepted April 10, 2018. Date of publication April 19, 2018; date of current version May 4, 2018. This work was supported in part by the National Natural Science Foundation of China under Grant 61571292 and Grant 61535006 and in part by the Shanghai Key Laboratory of Specialty Fiber Optics and Optical Access Networks STCSM under Grant SKLSFO2015-04. *(Corresponding author: Weiwen Zou.)*

The authors are with the State Key Laboratory of Advanced Optical Communication Systems and Networks, Department of Electronic Engineering, Shanghai Institute for Advanced Communication and Data Science, Shanghai Jiao Tong University, Shanghai 200240, China (e-mail: stendardo@sjtu.edu.cn; wzou@sjtu.edu.cn; qianna@sjtu.edu.cn; jpchen62@sjtu.edu.cn).

Color versions of one or more of the figures in this letter are available online at http://ieeexplore.ieee.org.

Digital Object Identifier 10.1109/LPT.2018.2828459

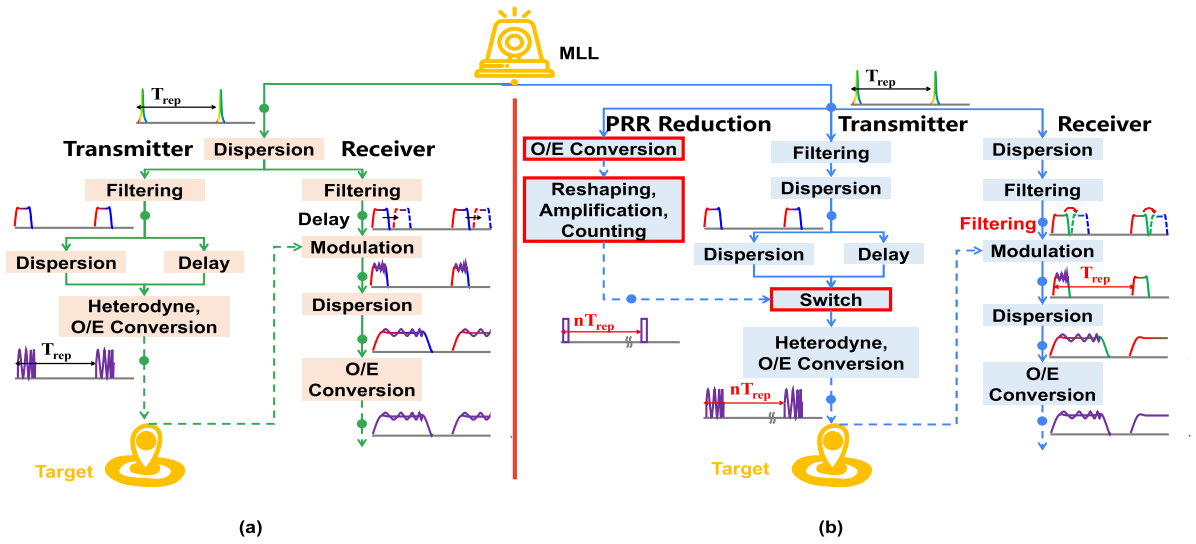

Fig. 1. Comparison of two schemes of PTS-MR. (a) The original scheme presented in [6]. The pulse repetition rate (PRR) of the MLL in the transmitter constrains the measurement range. The reception aperture is limited by the length of the delay line. (b) The novel scheme reported in this letter. The PRR in the transmitter is reduced by the photonic switch. The time-stretched aperture in the receiver is widely tunable by simply changing the center wavelength of the filter. MLL: mode-locked laser. O/E conversion: opto-electronic conversion.

The transmitted signal was reflected back by the target and modulated on the chirped optical pulse, of which the duration is called the reception aperture. Later, more dispersion was applied to the modulated pulses to carry out the time-stretched process. To guarantee a successful modulation, the reception aperture was tuned by a variable optical delay line with a finite length variation. Finally, the echo with the compressed bandwidth was detected by the O/E conversion.

In comparison, Fig. 1(b) depicts the schematic of the novel scheme. To enlarge the ambiguity-free measurement range, a small part of the optical pulses from the MLL is directly converted to microwave pulses. After the reshaping, amplification, and counting process, a synchronous gate pulse train with the reduced PRR is generated as the control signal of the photonic switch.

The electromagnetic field of the chirped optical pulses can be expressed as

$$E(t) = H\left(\lambda_0 + \frac{t}{\psi_2}\right) \cdot e^{-j\frac{t^2}{2\psi_2}} \quad \text{where} \quad -\frac{\Delta\lambda}{2} \le \frac{t}{\psi_2} \le \frac{\Delta\lambda}{2} \tag{1}$$

where λ_0 is the center wavelength of the optical filter, $H(\lambda)$ is the amplitude at the wavelength of λ, ψ_2 is the first-order dispersion value at λ_0, and $\Delta\lambda$ is the bandwidth of the optical filter.

Equation (1) denotes that the reference pulse timing can be tuned by simply changing the center wavelength of the optical filter [13]. If different wavelength components of MLL are filtered out to form the chirped optical pulse, the reception aperture is tunable. Therefore, the reception aperture can be tunable in sequence to cover the entire measurement range if specific center wavelengths of the chirped optical pulse are set and the high PRR of the MLL is maintained.

The experimental setup of the proposed scheme of PTS-MR is shown in Fig. 2. It consists of three parts: the transmitter, receiver, and PRR reduction. They share the same optical source by equally dividing it by an optical coupler (OC1). The optical source is an MLL (Precision Photonics Corp., FFL-1560-B) with tens of nanometer bandwidth and 37 MHz of the PRR. In order to reduce the PRR, the optical pulse train in the transmitter is partially divided by OC2 with the ratio of 10/90. The 90% branch of optical pulses is dispersed by the dispersion compensation fiber (DCF1), amplified by the erbium-doped fiber amplifier (EDFA1), and filtered by the tunable optical filter (TOF1, Alnair Labs, CVF-300CL). The dispersion coefficient of DCF1 is −985.5 ps/nm and the bandwidth of the TOF1 is 2 nm. The dispersed rectangular-shaped optical pulse with respect to time is equally split by OC3 to two arms. DCF2 adds extra dispersion with −23 ps/nm to the optical pulses in the upper arm. In the lower arm, a variable optical delay line (VODL, General Photonics, MDL-002)

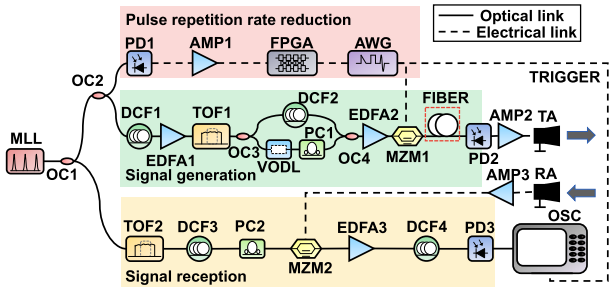

Fig. 2. Experimental setup of the proposed PTS-MR. MLL: mode-locked laser; OC: optical coupler; PD: photo-detector; AMP: amplifier; FPGA: field programmable gate array; AWG: arbitrary waveform generator; EDFA: erbium-doped fiber amplifier; TOF: tunable optical filter; DCF: dispersion compensation fiber; VODL: variable optical delay line; PC: polarization controller; MZM: Mach-Zehnder modulator; TA: transmitting antenna; RA: receiving antenna; OSC: oscilloscope. Note that the reference signal of the PTS-MR is recorded when a fiber segment (dashed rectangle) isn't inserted between the MZM1 and PD2.

is added to adjust the relative time delay between the pulses in those two arms for X-band signal generation. The polarization controller (PC1) in the lower arm is applied to increase the interference visibility.

After coupled together by OC4 and amplified by EDFA2 (Calmar, Coronado), the optical pulses are additionally modulated by MZM1 (Photline, MXAN-LN-40) to suppress the redundant pulses and reduce the PRR. The optical pulses in the 10% branch from OC2 is converted into the electric pulses by a photo-detector (PD1, EM4, EM169-03) and amplified by a microwave amplifier (AMP1, RF Bay, MPA-22-30). The field programmable gate array (FPGA, Xilinx, Spartan-6) receives the electric pulses and outputs a TTL-level signal for every ten counts to synchronize the arbitrary waveform generator (AWG, Agilent, 81150A). The AWG generates a rectangle-like pulse train with 3.7 MHz PRR to drive MZM1 served as a photonic switch. Finally, the PRR-reduced optical pulse train is converted into microwave pulses at X-band by another PD2 with 18 GHz bandwidth and amplified by AMP2 (RF Bay, LNA-14G).

Two antennas in the transmitter and receiver (TA and RA) are aligned side by side. AMP3 (RF Bay, LNA-14G) is added after RA to compensate the propagation loss. In the receiver, TOF2 (Alnair Labs, CVF-220CL) with 8 nm bandwidth is employed and DCF3 has a dispersion coefficient of 660.6 ps/nm. After filtered and dispersed, the chirped optical pulse has a reception aperture of ∼5.3 ns to sample the echoes via MZM2 (Photline, MXAN-LN-20). The sampled optical pulses are amplified by EDFA3 (Calmar, Coronado) and dispersed again by DCF4 for the time-stretched process. The dispersion coefficient of DCF4 is 2642.4 ps/nm. The nominal time-stretch factor is five. The envelope of the time-stretched optical pulses is transferred to electric pulses by PD3 with 3 GHz bandwidth and digitized by an oscilloscope (Lecroy, SDA 845Zi-A). The oscilloscope is triggered by the AWG output.

III. Results and Discussion

Fig. 3(a) shows the measured signal after PD1. The pulse period T_{rep} is ∼27 ns, corresponding to the PRR of 37 MHz. In Fig. 3(b), the dotted curve denotes the driving signal applied on MZM1 and the solid curve depicts the transmitted signal after the PRR reduction. Both of them are in good synchronization and the redundant pulses are well suppressed. The PRR of the signal is tenfold reduced from 37 MHz to 3.7 MHz, corresponding to an ambiguity-free measurement range of 40.5 m. Fig. 3(c) depicts the tunable reception aperture measured after EDFA3 in the reception part. Five different time segments correspond to different wavelength segment centered at 1534, 1542, 1550, 1558 and 1566 nm. The amplitude fluctuation is mainly caused by the uneven spectrum of the MLL. The tunable property of the reception aperture proves that the entire measurement can be covered.

The time and frequency characteristics of the generated and received signal is summarized in Fig. 4. Fig. 4(a) shows the temporal trace of the transmitted signal after TA. The time duration is ∼1.6 ns. The short time Fourier transform (STFT)

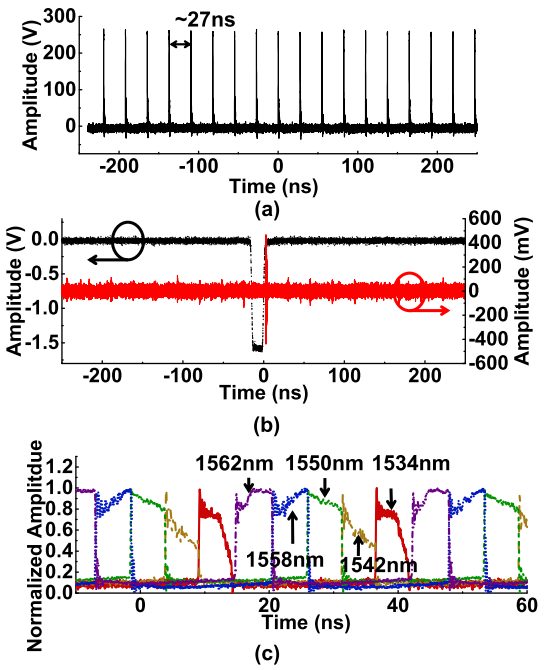

Fig. 3. (a) Measured signal after PD1. The PRR is ∼37 MHz. (b) Generated radar signal detected after AMP2 (solid curve). Dotted curve corresponds to rectangle-like pulse train from the AWG. (c) Optical pulses in the receiver detected before DCF4. Different traces correspond to different center wavelengths of 1534, 1542, 1550, 1558 and 1566 nm.

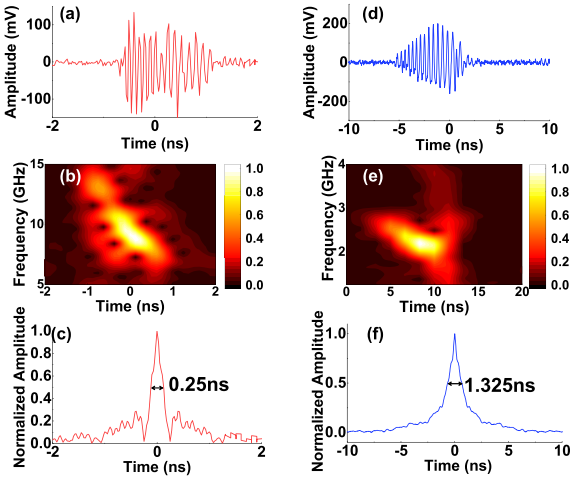

Fig. 4. (a) Temporal traces, (b) short time Fourier transform (STFT) analysis, and (c) autocorrelation of the transmitted signal. (d) Temporal traces, (e) STFT analysis, and (f) autocorrelation of the received signal after time-stretched process.

analysis in Fig. 4(b) verifies that the generated signal spans from 8 GHz to 12 GHz, covering the whole X band. The autocorrelation result shows that the compression ratio is 6.4 in Fig. 4(c), corresponding to the bandwidth of 4 GHz. The temporal trace of the received signal at PD3 is depicted in Fig. 4(d) and the signal lasts ∼8 ns in time domain. Fig. 4(e) shows the STFT analysis of the received signal. The autocorrelation result in Fig. 4(f) corresponds to the bandwidth of 0.75 GHz. Therefore, the time-stretch factor is calculated to be 4/0.75 = 5.33, which is a little larger than the nominal

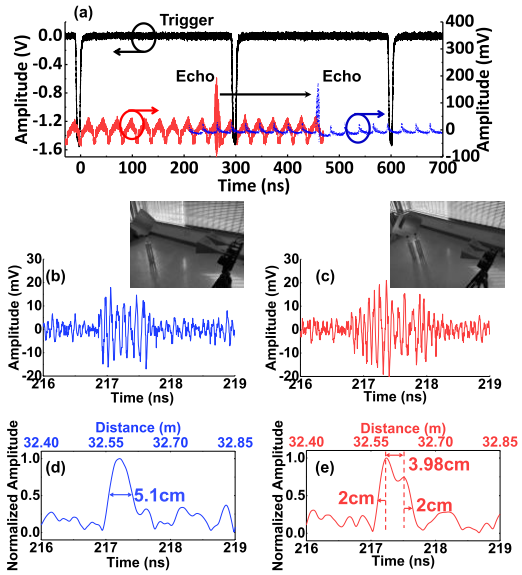

Fig. 5. Comparison of the detected echo with (dashed) or without (solid) the insertion of the fiber segement. The detected echo of one target (b) and two targets (c). Matched filtering process of the detected echo of one target (d) and two targets (e). The inset in (b) or (c) shows the experimental layout of the one-target or two-target detection.

one. The range resolution of the pulse compression radar is given by [2]

$$\delta_r = \frac{c}{2B} \tag{2}$$

where c is the velocity of the light and B the bandwidth of the transmitted signal in the radar. The theoretical expectation of the range resolution is ∼3.75 cm.

By setting TA and RA side by side, we testify the maintained resolution and the enhanced measurement range. Two 1-mm-thin metal flats with the sizes of 30 cm × 30 cm are placed away as targets. Due to the limitation of the laboratory size, the targets are set ∼1 m away from the antennas and a ∼42-meter-long fiber is inserted before PD2 to approximate the measurement distance between the transmitter and receiver of PTS-MR. As depicted in Fig. 5(a), the relative time delay to the trigger signal is increased by about 200 ns. The echoes of one target and two targets are measured after PD3, respectively. Subtraction between the optical pulses with and without the echo modulation is used to eliminate the influence of the pulse envelope [6]. Fig. 5(b) shows the echo of one target. After the matched filtering process [6], one target at the distance of 32.58 m is identified with the resolution of 5.1 cm as shown in Fig. 5(e).The distance corresponds to the radar's one-way transmitting distance from the targets to the transmitter or receiver antenna, which includes the optical path difference introduced by the fiber inserted before PD2. Fig. 5(c) illustrates the received echo of two neighboring targets. As depicted in Fig. 5(e), two targets separated by 3.98 cm are distinguishable after the matched filtering process. The detection resolution is consistent with the theoretical expectation of ∼3.75 cm.

IV. Conclusion

We have presented a novel scheme of PTS-MR. The measurement range of the scheme is tenfold enhanced by reduction of the PRR of the optical pulse in the transmitter; the reception aperture for the time-stretched process is ensured to be tuned in sequence by changing the central wavelength of the optical filter laid in the receiver. The proof-of-concept experiment has testified that the novel scheme possesses the resolution of ∼4 cm and the measurement range of more than 40 m although the PRR of the MLL served as the laser source of PTS-MR is 37 MHz. For more practical application, we are now planning to increase the time duration of the broadband transmitted signal [14] and reduce the PRR by more times in the transmitter of the PTS-MR.

References

[1] J. D. McKinney, "Technology: Photonics illuminates the future of radar," *Nature*, vol. 507, pp. 310–312, Mar. 2014.
[2] W. L. Melvin and J. A. Scheer, *Principles of Modern Radar*. Edison, NJ, USA: SciTech Publishing, 2014.
[3] J. Scheer and J. L. Kurtz, *Coherent Radar Performance Estimation*, Norwood, MA, USA: Artech House, 2012.
[4] J. Capmany and D. Novak, "Microwave photonics combines two worlds," *Nature Photon.*, vol. 1, no. 6, pp. 319–330, Apr. 2007.
[5] P. Ghelfi *et al.*, "A fully photonics-based coherent radar system," *Nature*, vol. 507, no. 7492, pp. 341–345, Mar. 2014.
[6] W. Zou, H. Zhang, X. Long, S. Zhang, Y. Cui, and J. Chen, "All-optical central-frequency-programmable and bandwidth-tailorable radar," *Sci. Rep.*, vol. 6, no. 1, Jan. 2016, Art. no. 19786.
[7] R. Li *et al.*, "Demonstration of a microwave photonic synthetic aperture radar based on photonic-assisted signal generation and stretch processing," *Opt. Exp.*, vol. 25, no. 13, pp. 14334–14340, Jun. 2017.
[8] F. Zhang *et al.*, "Photonics-based broadband radar for high-resolution and real-time inverse synthetic aperture imaging," *Opt. Exp.*, vol. 25, no. 14, pp. 16274–16281, Jun. 2017.
[9] X. Xiao *et al.*, "A microwave photonics-based inverse synthetic aperture radar system," in *Proc. Conf. Lasers Electro-Opt.*, May 2017, p. JW2A-144.
[10] H. Gao, C. Lei, M. Chen, F. Xing, H. Chen, and S. Xie, "A simple photonic generation of linearly chirped microwave pulse with large time-bandwidth product and high compression ratio," *Opt. Exp.*, vol. 21, no. 20, pp. 23107–23115, Oct. 2013.
[11] Y. Li, A. Rashidinejad, J.-M. Wun, D. E. Leaird, J.-W. Shi, and A. M. Weiner, "Photonic generation of W-band arbitrary waveforms with high time-bandwidth products enabling 3.9 mm range resolution," *Optica*, vol. 1, no. 6, pp. 446–454, 2014.
[12] H. Zhang, W. Zou, and J. Chen, "Generation of a widely tunable linearly chirped microwave waveform based on spectral filtering and unbalanced dispersion," *Opt. Lett.*, vol. 40, no. 6, pp. 1085–1088, Mar. 2015.
[13] A. Mahjoubfar, D. V. Churkin, S. Barland, N. Broderick, S. K. Turitsyn, and B. Jalali, "Time stretch and its applications," *Nature Photon.*, vol. 11, no. 6, pp. 341–351, Jun. 2017.
[14] S. Zhang, W. Zou, K. Wu, and J. Chen, "Duration expansion of wavelength-to-time mapping based on a programmable dispersion loop," in *Proc. Photon. Global Conf. (PGC), Opto-Electron. Commun. Conf. (OECC)*, Singapore, Jul./Aug. 2017, pp. 1–3.